

Spin properties of very shallow nitrogen vacancy defects in diamond

B. K. Ofori-Okai,¹ S. Pezzagna,² K. Chang,³ M. Loretz,³ R. Schirhagl,³ Y. Tao,^{1,3} B. A. Moores,³ K. Groot-Berning,² J. Meijer,² and C. L. Degen^{3,*}

¹*Department of Chemistry, Massachusetts Institute of Technology, 77 Massachusetts Avenue, Cambridge, Massachusetts 02139, USA*

²*RUBION, Ruhr-Universität Bochum, Universitätsstrasse 150, 44780 Bochum, Germany*

³*Department of Physics, ETH Zurich, Schafmattstrasse 16, 8093 Zurich, Switzerland*

(Received 4 January 2012; revised manuscript received 1 August 2012; published 13 August 2012)

We investigate spin and optical properties of individual nitrogen vacancy centers located within 1–10 nm from the diamond surface. We observe stable defects with a characteristic optically detected magnetic-resonance spectrum down to the lowest depth. We also find a small but systematic spectral broadening for defects shallower than about 2 nm. This broadening is consistent with the presence of a surface paramagnetic impurity layer [Tisler *et al.*, *ACS Nano* **3**, 1959 (2009)] largely decoupled by motional averaging. The observation of stable and well-behaved defects very close to the surface is critical for single-spin sensors and devices requiring nanometer proximity to the target.

DOI: [10.1103/PhysRevB.86.081406](https://doi.org/10.1103/PhysRevB.86.081406)

PACS number(s): 76.30.Mi, 75.70.Cn, 68.35.Dv, 76.70.Hb

Isolated defect spins in solids, such as phosphorus donors in silicon¹ or the nitrogen vacancy (NV) center in diamond,² are considered important building blocks for future nanoscale devices, governed by quantum mechanics. In pure materials, defects can be so well decoupled from their solid host that spin states approach a stability normally only found in dilute atomic vapors, including coherence times of milliseconds to seconds.^{3,4} Not surprisingly, atomic defects have over the last decade attracted increasing attention motivated by their potential for spin qubits in quantum information^{5,6} or for ultrasensitive magnetic detectors with nanometer spatial resolution.^{7–9}

The central challenge with many of these endeavors is to position the defect of interest in close proximity to other circuit elements while retaining their well-defined properties known from the bulk. On the one hand, close proximity is required for strong-enough coupling. For example, for the direct coupling to nearby spin magnetic dipoles—which scales as r^{-3} , where r is the distance—efficient coupling is only achieved at nanometer separations. Furthermore, for scanning magnetometry applications, r directly sets the attainable spatial resolution.⁷ On the other hand, the coupling will almost always happen across a material interface and defects will have to be located within nanometers from a surface, potentially destabilizing the spin and limiting its usefulness.

Several mechanisms have been found or proposed to affect the stability of shallow defects. For single donor spins in silicon, for example, the nearby Si/SiO₂ interface was shown to decrease spin coherence times even for donors tens of nanometer away due to paramagnetic impurities present at the interface.¹⁰ Other possible mechanisms include electric surface charge or strain fluctuations that may disturb defects through Stark and spin-orbit effects, or direct ionization.^{11,12} For nitrogen vacancy centers in diamond, on the other hand, rather little is currently known about the spin's performance near the surface. While functional defects have recently been reported in <10-nm-diameter nanocrystals^{13,14} and within 3–4 nm from bulk diamond surfaces,¹⁵ and coherence times T_2 of tens of μ s have been observed for defects at \sim 10 nm proximity,^{16–18} neither a “shallowest depth” nor the involved

destabilizing mechanisms are known. Given the fundamental importance of surface proximity for applications, it appears imperative to experimentally explore the limits to stability of defects at very shallow depths.

Here we report a systematic study of the spin resonance properties of single NV defect centers down to a proximity of about 1 nm. Defects were produced by low-energy ion implantation (0.4–5 keV) and investigated by optically detected magnetic-resonance (ODMR) spectroscopy. We find well-behaved defects exhibiting a narrow electron spin resonance (ESR) spectrum and coherence times exceeding 10 microseconds down to the shallowest investigated depths. We also observe extra line broadening for defects shallower than 2 nm. This broadening is compatible with the presence of surface magnetic impurities that are mostly decoupled from the NV spin by motional averaging.

A (100)-oriented single crystal of ultrapure diamond (<5 ppb N concentration, element six) was used as the sample for all experiments. One sample face was implanted with ¹⁵N⁺ or ¹⁵N₂⁺ ions at a series of very low energies (0.4–5 keV, in steps of 0.2 keV) and fluences (10^{10} – 10^{14} N/cm²)^{19,20} (see Fig. 1). To form NV centers, the sample was annealed for 2 h at 800 °C and $p < 2 \times 10^{-7}$ mbar. It is expected that nitrogen atoms do not diffuse at these temperatures because the activation energy is too high.^{21–23} The sample was cleaned by boiling it for 24 h under reflux in a 1:1:1 mixture of sulfuric, nitric, and perchloric acid and thoroughly rinsed with purified water.¹³ This procedure is known to remove any residues (such as graphite) but to leave the diamond *sp*³ bonding network intact. Acid treatment also leaves a well-defined, oxygen-terminated reference surface.¹³ Additional details on implantation and sample preparation are given as Supplemental Material.²³

We have performed a detailed inspection of the prepared diamond surface to validate the sample for later spin resonance measurements. Surface roughness was determined by atomic force microscopy and was found to be very low ($x_{\text{rms}} = 0.38$ nm, over a 300×300 nm² window) compared to the defect depth (>1 nm). Angle-resolved x-ray photoelectron spectroscopy (ARXPS) was used to confirm oxygen termination of the surface and the absence of significant graphite

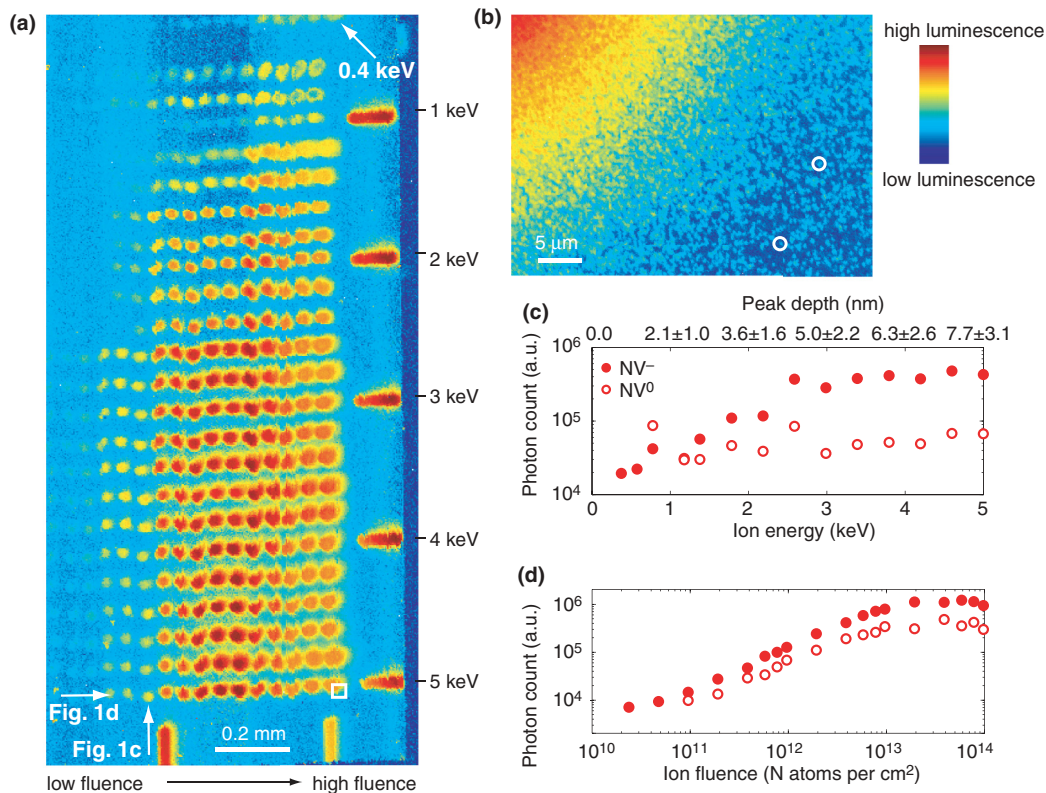


FIG. 1. (Color online) (a) Photoluminescence intensity map of the diamond surface. Shallowest 0.4 keV defects are visible at the very top. The excitation wavelength was 532 nm and the detection bandwidth was 630–800 nm for all experiments except (c) and (d). (b) Close-up of an implantation spot at 5.0 keV [white square in (a)]. Some single NV centers are encircled. (c) Luminescence intensity due to NV⁻ (full circles) and NV⁰ (empty circles) as a function of ion energy at a fluence of $8 \times 10^{11} \text{ cm}^{-2}$, measured using two pairs of filters and corrected for spectral overlap.^{12,23} (d) Luminescence intensity as a function of ion fluence at an energy of 5 keV.

residue. The absence of sp^2 carbon was further corroborated by confocal Raman spectroscopy. No difference was found between implanted and nonimplanted regions.

A photoluminescence intensity map of the sample is shown in Fig. 1(a). Most prominently, we observe that optically bright NV centers are visible down to the lowest implantation energy (0.4 keV). We have estimated the depth of these defects using stopping range of ions in matter (SRIM) Monte Carlo simulations;^{23,24} for example, an energy of 0.4 keV corresponds to a peak depth of $1.1 \pm 0.6 \text{ nm}$ [see scale in Fig. 1(c)]. The advantage of SRIM calculations, which is the primary method to determine defect depths in this study, is that they give suitable results of ion implantation depths over a wide energy range, including very low implantation energies.²⁵ This is important given the current lack of a precise experimental method to directly measure surface proximity. The drawbacks of SRIM calculations are that the results are inherently statistical (which is addressed below by collecting statistics on many defects) and important biasing effects like channeling are not considered. We have analyzed these effects for our study (see Supplemental Material). In particular, we find that ion channeling, which could lead to depth underestimation by about a factor of 2,^{22,26} does not occur for ¹⁴N energies below 0.6 keV and is only important towards higher energies.²³ The lowest energies, where channeling is absent, are the most relevant in this study.

Figures 1(c) and 1(d) provide additional photoluminescence data that further corroborates this picture. We have measured the total photoluminescence intensity both as a function of energy and ion fluence and determined the relative concentrations of NV⁻ and NV⁰ centers. In good agreement with earlier studies carried out at higher energies,¹⁹ we find a monotonic decrease in total photoluminescence with decreasing energy. This decrease has been attributed to the vacancy-limited formation of NV centers.¹⁹ Since the decrease appears to be mostly due to a reduction of NV⁻, one could conjecture the presence of a depth threshold below which the negative charge state becomes unstable.¹² We have not, however, observed any photobleaching and we have only seen a few rare cases of fluorescence intermittency among the investigated single centers¹⁴ that would support such a threshold. The presence of a threshold is also incompatible with the rapid changes in the spin resonance linewidth that we see for the lowest energies (see below).

We now turn to the core part of this Rapid Communication, which is a study and analysis of electron spin resonance (ESR) spectra as a function of defect depth. ESR measurements are carried out using optically detected magnetic-resonance spectroscopy.²⁷ For these measurements, the fluorescence intensity from a single, isolated NV center is collected, while slowly sweeping an auxiliary cw microwave field across the spin resonance ($\sim 2.8 \text{ GHz}$) of the electronic ground state.

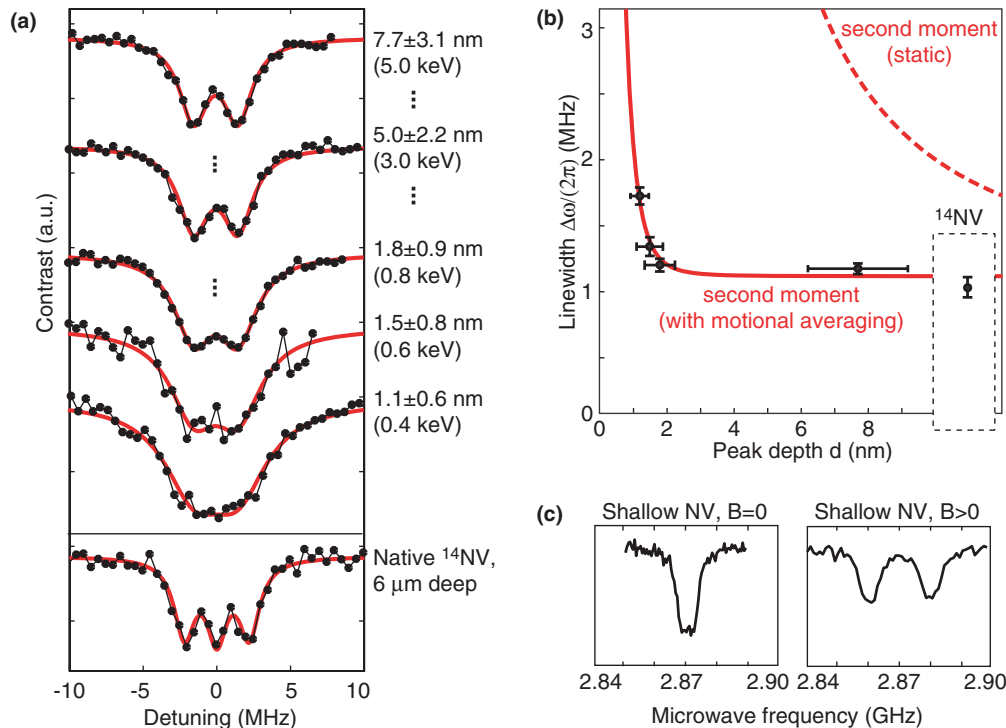


FIG. 2. (Color online) Electron spin resonance measurements on shallow NV defect spins. (a) Representative spectra (out of >30 total) showing increased line broadening at shallow depths. Black dots are experimental points and red solid lines are Lorentzian fits. Implanted ^{15}N (nuclear spin $I = 1/2$) are distinguished from native ^{14}N ($I = 1$, 99.6% natural abundance) by the different hyperfine manifold. The magnetic bias field is about 20 gauss. (b) ESR linewidth $\Delta\omega/2\pi$ (half width at half height) plotted against surface proximity d . Black dots are experimental values obtained from many separately fitted curves, such as the ones shown in (a). Error bars denote standard error. The solid red line is a fit to the black dots based on Eq. (2) including motional averaging. The dashed red line is the static second moment [Eq. (1)] shown for comparison. The linewidth of reference ^{14}N is also shown. (c) Spectra of a 1.1 nm defect at zero field (left) and at 3.5 gauss bias field (right) rule out the presence of significant surface strain or charge (see text).

Resonant microwaves induce transitions between the $m_s = 0$ and $m_s = +1$ (or $m_s = -1$) spin sublevels and lead to an up to 30% reduction in fluorescence. We use this feature to map out ESR spectra of single defects and to measure their linewidth and coherence properties.

Figure 2(a) collects a series of representative ESR spectra taken on NV centers at different depths. As a key feature, we observe increased line broadening as NV spins are located closer to the surface: For defects deeper than 1.8 nm (0.8 keV), there is a clear hyperfine splitting due to the ^{15}N nuclear spin, but for the shallower defects at 1.5 nm (0.6 keV) and 1.1 nm (0.4 keV), the resonances become broad and the hyperfine doublet is barely visible or entirely unresolvable. This picture of broadened lines was consistent among recorded spectra (>30 in total); for example, we did not find any 0.4 keV defects with a resolved hyperfine splitting, while most 0.8 keV and virtually all deeper defects showed a clear hyperfine doublet.

We have quantitatively analyzed the linewidth for the shallowest defects (where the pronounced changes are seen) by collecting and fitting a number of individual spectra and averaging the resultant linewidth parameter [Fig. 2(b)]. While we have taken additional spectra at other (higher) energies that all show clear hyperfine doublets, these spectra do not have statistical significance and are not included in the figure. Spectra are recorded at a single fluence ($8 \times 10^{11} \text{ cm}^{-2}$) and on

defects that lie at the perimeter of an implantation dot, where the density is low enough to optically isolate individual NV centers and residual dipolar broadening by N donor electronic spins can be excluded.²³

Several control measurements were carried out to ensure that the observed line broadening is indeed a result of surface proximity. A number of native ^{14}N spectra was recorded at each investigated implantation spot by focusing slightly into the bulk in order to verify that broad lines were a property of the defect, and not, e.g., the sample or experimental parameters. We have also measured a few spectra at higher fluence (up to $1 \times 10^{13} \text{ cm}^{-1}$) and found that the line broadening did not change between implantation spots of the same energy but different fluence. Moreover, no increase in ^{14}N density is seen on or near implanted areas, which eliminates the possibility that ^{14}N centers were formed from vacancies created during ^{14}N implantation, in agreement with previous reports.²² Finally, we did not observe a line splitting at zero magnetic bias field [Fig. 2(c)], a signature for the presence of electric fields,²⁸ thereby excluding the presence of significant surface strain or charge.

In the following, we attempt to explain the surface-induced line broadening by the presence of paramagnetic impurities. Surface impurities have been found at substantial density for clean, oxygen-terminated nanodiamonds.¹³ These nanodiamonds were milled from larger crystals and underwent

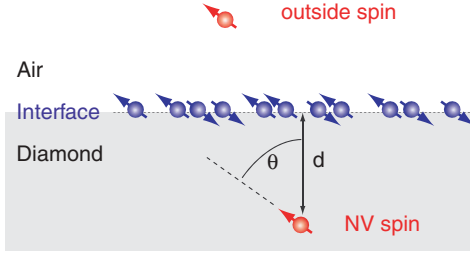


FIG. 3. (Color online) Sketch of a nitrogen vacancy defect spin near a paramagnetic surface impurity layer, as described in the text. d and θ denote distance and orientation, respectively, of the defect spin to the interface plane, and quantization is along the NV axis. A potential target spin, representative for sensing applications, is also shown.

the same surface cleaning procedure, and are thus expected to exhibit a surface chemistry very similar to our diamond substrate. We can model surface impurities by assuming a homogeneous, two-dimensional dipolar bath of electron spins ($S = 1/2$) with an areal density of $\rho_A \approx 10$ spins/nm²,¹³ similar to the sketch in Fig. 3. In the following, we use the theory of moments,²⁹ but note that a parallel framework has been developed for T_1 and T_2 values in the context of paramagnetic impurities in the Si/SiO₂ interface.¹⁰ The second moment $\langle \Delta\omega^2 \rangle_d$ ($\langle \Delta\omega^2 \rangle_d \approx \Delta\omega_d^2$, where $\Delta\omega_d$ is linewidth) of the NV spin resonance at a distance d from the spin bath is found to be

$$\langle \Delta\omega^2 \rangle_d = \frac{3\hbar^2 \mu_0^2 \rho_A \gamma^4}{2048\pi d^4} (3 + 2\cos^2\theta + 3\cos^4\theta), \quad (1)$$

where $\mu_0 = 4\pi \times 10^{-7}$ Vs/(Am), $\gamma/(2\pi) = 2.8 \times 10^{10}$ Hz/T is the surface electron gyromagnetic ratio, and θ is the angle between the NV axis and surface normal.²³ For an NV center near a (100) surface ($\theta = 54.7^\circ$), the angular factor in Eq. (1) $3 + \cos^2\theta + 3\cos^4\theta = 4$. The resonance linewidth that can be directly compared to the experiment is then $\Delta\omega = \sqrt{\Delta\omega_0^2 + \langle \Delta\omega^2 \rangle_d}$, where $\Delta\omega_0$ is the intrinsic linewidth [here $\Delta\omega_0/(2\pi) = 1.1 \pm 0.1$ MHz].

Equation (1) describes the second moment of a quasistatic spin bath that does not fluctuate on the time scale of the NV dephasing time, $T_2^* \approx \Delta\omega^{-1/2}$. This assumption is likely invalid for surface spins that are not protected by the

diamond matrix. For example, spin-lattice relaxation times T_1 observed for paramagnetic impurities in amorphous carbon³⁰ and sintered detonation nanodiamonds³¹ are on the order of nanoseconds. Following the work by Kubo and Tomita,³² we can calculate a modified second moment that takes into account fast fluctuations (“motional averaging”),

$$\langle \Delta\omega^2 \rangle'_d = (\langle \Delta\omega^2 \rangle_d \tau_c)^2, \quad (\tau_c \ll \langle \Delta\omega^2 \rangle_d^{-1/2}), \quad (2)$$

where $\tau_c \approx T_{1,\text{surface spins}}$ is the correlation time of fluctuations.

We can compare the model represented by Eqs. (1) and (2) through a fit to the experimental data in Fig. 2(b). The three experimental parameters are the surface spin density ρ_A , the distance d , and the correlation time τ_c . Assuming $\rho_A = 10$ spins/nm² (Ref. 13) and d from the SRIM calculation,²³ one obtains a correlation time $\tau_c < 1$ ns. This τ_c would be rather fast compared to the above literature values^{30,31} and typical organic radicals. As neither ρ_A nor d are accurately known, our value for τ_c is at best approximate. For example, if we allow ρ_A to vary between 0.1–10 spins/nm² and assume an underestimation of depth d by up to 2 times, then the range of compatible τ_c varies between 0.1–100 ns. Further evidence for a correlation time τ_c in the nanosecond range comes from relaxation-time measurements on selected shallow defects where we observe $T_1 \gg T_{1\rho} \approx T_2$.³³

Finally, we have also measured echo-decay times of several 0.4 keV (1.1 nm) defects to establish a lower bound for the coherence times T_2 of very shallow spins. A representative Hahn echo-decay curve with an echo-decay time of $\tau = 12 \mu\text{s}$ is shown in Fig. 4; other defects at the same depth showed τ values between 7 and 12 μs . We note that the echo-decay profile is Gaussian, which is expected if decay is caused by the slowly fluctuating ¹³C nuclear-spin environment. If echo decay were set by rapidly fluctuating surface impurities, then one would rather expect an exponential decay. Consequently, one can conclude that surface spins are not the dominant source of decoherence and that the limit on T_2 implied by surface impurities is $\sim 10 \mu\text{s}$.

Given the shallow depths of the investigated NV centers, it is instructive to extrapolate their magnetic-moment sensitivity, which is the key figure of merit for the sensing of external spins and future applications to nanoscale magnetic-resonance imaging and spectroscopy.⁷ For example, taking an echo-decay time $\tau \sim 12 \mu\text{s}$, a photon count rate of

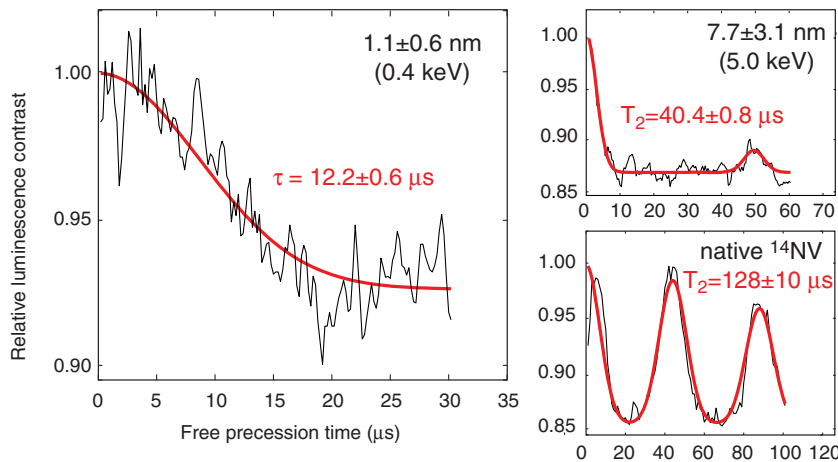


FIG. 4. (Color online) Hahn echo decay of a 1.1 nm ¹⁵NV center and, for comparison, for a 7.7 nm ¹⁵NV and a native ¹⁴NV defect. Black curves are experimental data and red lines are fits. The fit function is given in Ref. 23.

$C = 0.0018$ photons/shot, and an optical contrast between $m_s = 0$ and $m_s = \pm 1$ states of $\epsilon = 7\%$ (1.1 nm defect in Fig. 4), we find an optimal ac magnetic field sensitivity of $B_{\min} \approx (0.5\pi\gamma\epsilon\sqrt{\tau C})^{-1} \sim 2.2 \mu\text{T}/\sqrt{\text{Hz}}$.³⁴ Here, the relevant (most susceptible) ac frequency is set by the inverse of the echo duration, i.e., tens of kHz. For a magnetic moment located directly on the surface and taking into account the angle of the NV spin, this sensitivity equates to a minimum detectable magnetic moment of $\mu_{\min} \sim B_{\min}/[(0.96 \times \mu_0\mu_B)/(4\pi d^3)] \sim 0.003 \mu_B/\sqrt{\text{Hz}}$, where μ_B is the Bohr magneton. For dc signal detection, the corresponding magnetic field and moment sensitivities are $B_{\min} \approx 8\Delta\omega_0/(3\sqrt{3}\gamma\epsilon\sqrt{I_0}) \sim 19 \mu\text{T}/\sqrt{\text{Hz}}$ and $\mu_{\min} \sim 0.03 \mu_B/\sqrt{\text{Hz}}$, respectively, where $I_0 = 2 \times 10^3$ photons/s is the cw photon count rate and $\epsilon = 11\%$ [Fig. 2(a)]. Even if our depth was underestimated by a factor of 2,²³ μ_{\min} would still equate to $0.03 \mu_B/\sqrt{\text{Hz}}$ (ac) and $0.2 \mu_B/\sqrt{\text{Hz}}$ (dc), respectively.

In conclusion, we have investigated spin and optical properties of single nitrogen vacancy defects in diamond at very shallow depths. Functional defects are found down to about 1 nm, and significant broadening of the electron spin

resonance is only observed for defects < 2 nm. This surface stability is unmatched by other solid-state spin systems, such as phosphorus donors in silicon or semiconductor quantum dots, and is a key requirement for a number of anticipated quantum and sensing applications. In particular, we have inferred a sensitivity to outside magnetic moments (such as surface electron and nuclear spins) that extends down to $< 0.01 \mu_B/\sqrt{\text{Hz}}$. To the best of our knowledge, this is the best magnetic-moment sensitivity demonstrated for a general-purpose magnetic sensor to date.³⁵ If combined with the imaging capabilities of a scanning probe apparatus,^{7,36} this sensitivity will enable the direct mapping of nuclear spins in molecules and thin films with chemical specificity and nanometer spatial resolution.

The authors gratefully acknowledge financial support through the NCCR QSIT, a competence center funded by the Swiss NSF, through SNF Grant No. 200021_137520/1, and through the Volkswagen Stiftung. We thank G. Balasubramanian, H. Balch, J. Hodges, L. Robledo, and C. Ryan for support in constructing the optical setup, and A. Rossi and J. Stadler for help with the surface inspection.

*degenc@ethz.ch

¹G. Feher, *Phys. Rev.* **114**, 1219 (1959).

²F. Jelezko and J. Wrachtrup, *Phys. Status Solidi A* **203**, 3207 (2006).

³G. Balasubramanian *et al.*, *Nature Mater.* **8**, 383 (2009).

⁴A. M. Tyryshkin *et al.*, *Nature Mater.* **11**, 143 (2012).

⁵B. Kane, *Nature (London)* **393**, 133 (1998).

⁶D. D. Awschalom, R. Epstein, and R. Hanson, *Sci. Am.* **297**, 84 (2007).

⁷C. L. Degen, *Appl. Phys. Lett.* **92**, 243111 (2008).

⁸J. R. Maze *et al.*, *Nature (London)* **455**, 644 (2008).

⁹G. Balasubramanian *et al.*, *Nature (London)* **455**, 648 (2008).

¹⁰R. de Sousa, *Phys. Rev. B* **76**, 245306 (2007).

¹¹X. Hu and S. Das Sarma, *Phys. Rev. Lett.* **96**, 100501 (2006).

¹²L. Rondin *et al.*, *Phys. Rev. B* **82**, 115449 (2010).

¹³J. Tisler *et al.*, *ACS Nano* **3**, 1959 (2009).

¹⁴C. Bradac *et al.*, *Nature Nanotechnol.* **5**, 345 (2010).

¹⁵B. Grotz *et al.*, *New J. Phys.* **13**, 055004 (2011).

¹⁶T. Gaebel *et al.*, *Nature Phys.* **2**, 408 (2006).

¹⁷P. C. Maurer *et al.*, *Nature Phys.* **6**, 912 (2010).

¹⁸M. S. Grinolds *et al.*, *Nature Phys.* **7**, 687 (2011).

¹⁹S. Pezzagna, B. Naydenov, F. Jelezko, J. Wrachtrup, and J. Meijer, *New J. Phys.* **12**, 065017 (2010).

²⁰The use of molecular N_2^+ ions was necessary to access the lowest energies (≤ 2.4 keV). No difference has been found between N^+ or N_2^+ implanted defects either in this or in an earlier study (Ref. 19).

It is assumed that as the N_2^+ ion impinges the surface, the molecule breaks, sending two N atoms into the bulk.

²¹K. T. Koga, J. A. van Orman, and M. J. Walter, *Phys. Earth Planet. Inter.* **139**, 35 (2003).

²²D. M. Toyli, C. D. Weis, G. D. Fuchs, T. Schenkel, and D. D. Awschalom, *Nano Lett.* **10**, 3168 (2010).

²³See Supplemental Material at <http://link.aps.org/supplemental/10.1103/PhysRevB.86.081406>.

²⁴J. F. Ziegler, J. P. Biersack, and M. D. Ziegler, SRIM, the Stopping and Range of Ions in Matter, <http://srim.org> (unpublished).

²⁵P. Honicke *et al.*, *Anal. Bioanal. Chem.* **396**, 2825 (2010).

²⁶K. Nordlund (private communication).

²⁷A. Gruber *et al.*, *Science* **276**, 2012 (1997).

²⁸F. Dolde *et al.*, *Nature Phys.* **7**, 459 (2011).

²⁹C. P. Slichter, *Principles of Magnetic Resonance*, 3rd ed. (Springer, Berlin, 1990), p. 80.

³⁰R. C. Barklie, M. Collins, and S. R. P. Silva, *Phys. Rev. B* **61**, 3546 (2000).

³¹P. G. Baranov *et al.*, *Small* **7**, 1533 (2011).

³²R. Kubo and K. Tomita, *J. Phys. Soc. Jpn.* **9**, 888 (1954).

³³M. Loretz (unpublished).

³⁴J. M. Taylor *et al.*, *Nature Phys.* **4**, 810 (2008).

³⁵C. L. Degen, *Nature Nanotech.* **3**, 643 (2008).

³⁶B. M. Chernobrod and G. P. Berman, *J. Appl. Phys.* **97**, 014903 (2005).